Title: Novel preclinical model of human lung cancer cachexia: evidence for early adipose tissue wasting

Author List: Deena B. Snoke[1,5], Jos L. van der Velden[2,5], Emma R. Bellafleur[1,5], Jacob S. Dearborn[4,5], Sean M. Lenahan[2,5], Skyler C. J. Heininger[1], Jennifer L. Ather[1], Hailey Sarausky[2,5], Daniel Stephenson[6], Julie A. Reisz[6], Angelo D'Alessandro[6], Devdoot Majumdar[4,5], Yvonne M.W. Janssen-Heininger[2,5], Matthew E. Poynter[1], David J. Seward[2,5], and Michael J. Toth[1,3,5]

Affiliations: Departments of [1]Medicine, [2]Pathology and Laboratory Medicine, [3]Molecular Physiology and Biophysics, and [4]Surgery, and [5]University of Vermont Cancer Center, University of Vermont College of Medicine; [6]Department of Biochemistry and Molecular Genetics, University of Colorado Anschutz Medical Campus, Aurora, CO, USA.

Corresponding Author: Michael J. Toth, Ph.D.
Health Science Research Facility 126B
149 Beaumont Avenue
Burlington VT, 05405
Email : Michael.Toth@med.uvm.edu
Tele : (802)-656-7989
Fax : (802)-656-0747

Keywords: Lung neoplasms, cachexia, organoids, conditioned culture media, adipocytes, gene expression profiling, cytokines, adipose tissue, skeletal muscle, lipolysis

Abstract

Background: Cancer cachexia (CC), a syndrome characterized by skeletal muscle and adipose tissue wasting, reduces responsiveness to therapies and increases morbidity and mortality. Lung cancer is the leading cause of cancer-related deaths worldwide with a large percentage of patients experiencing CC. Despite a wealth of mechanistic data on CC, there are no approved treatments, which may relate to the fact that many pre-clinical models do not reproduce the pathophysiological features of human CC.

Methods: We generated tamoxifen-inducible, club cell specific *Kras*$^{G12D/+}$ (*G12D*) mice to model lung cancer and investigated the development and progression of CC by assessing tumor characteristics, time course of CC, adipose and skeletal muscle tissue sizes and transcriptional profiles, and circulating inflammatory cytokines.

Results: Induction of the *Kras*^{G12D} allele caused adenocarcinomas in the terminal bronchioles, which were evident at initiation of weight loss (10.5 ± 1.1% lung volume at 6 weeks). Weight loss in *G12D* mice averaged 15% over 12 weeks, with loss of both adipose (-72%-85% vs. WT) and skeletal muscle tissue mass (-17-23% vs. WT) and tissue transcriptional profiles consistent with CC. Exploiting the protracted time course of this model, we found that early during CC adipose tissue, but not skeletal muscle, mass and cell size were reduced by greater than 50% in *G12D* mice compared to WT, a result that was confirmed in a more rapidly progressive, *Kras* driven model of lung CC containing *Stk11* loss of function (*Kras*$^{G12D/+}$/*Stk11*$^{-/-}$) where depletion of adipose depots (>50% vs WT) occurred over 3.5 weeks. *G12D* mice showed circulating metabolomic markers of increased fat mobilization/utilization, including elevated glycerol levels (+20% vs. WT), which was also apparent in patients with lung cancer (+79% vs. non-cancer controls). Additionally, 3T3-L1 adipocytes treated with conditioned media (CM) from tumor organoids developed from *G12D* mice caused a 3-fold increase in glycerol and 2-3 fold increase in pro-inflammatory cytokine release compared to CM from WT lung tissue.

Conclusions: *G12D* mice develop CC over a more protracted period and phenocopy tumor and tissue cellular, mutational, transcriptomic, and metabolic characteristics relevant to human lung CC. Additionally, *G12D* mice show early loss of adipose tissue, and factors released from *G12D* lung tumor organoids produce metabolic adaptations *in vitro* that promote adipose tissue wasting. Thus, *G12D* mice model features of human lung CC and may advance the study of the pathoetiology and treatment of CC.

Introduction

Cancer cachexia (CC) is characterized by unintentional loss of body weight secondary to skeletal muscle and/or adipose tissue wasting [1] and is associated with treatment-related toxicities, poor response to chemo- and immunotherapies and increased morbidity and mortality [2-6]. Animal models have served as the basis for knowledge of the pathophysiology of CC and the development of therapeutics [7] because the syndrome typically occurs in later-stage disease, when patients are limited in their ability or willingness to participate in research. While these models have generated a wealth of data [7], there are currently no effective, approved treatments for CC. This lack of translation of pre-clinical evidence into treatments may be explained, in part, by the fact that current models do not mimic human CC [8-14]. Development of new CC models that better replicate the human condition with respect to tumor location and burden, temporal progression, and metabolic features are needed to identify tumor-host interactions that initiate CC to develop more effective therapies.

Lung cancer is the second most common cancer worldwide and the leading cause of cancer-related deaths [15]. A majority of patients with lung cancer exhibit signs of CC at diagnosis [16, 17], and patients with lung CC have lower mean survival time and are less responsive to chemo- and immunotherapies [6, 18]. Most preclinical data on lung CC are derived from the murine Lewis lung carcinoma (LLC) model. In this model, tumor cells are typically injected subcutaneous and grow rapidly, with weight loss beginning when the tumor reaches ~5% of body weight and mice progressing to cachexia in 2-3 weeks [19]. Neither the tumor growth or size nor the rate of weight loss of this model reflect lung CC in patients [20]. Thus, new models of lung CC need to be developed that better emulate the human condition.

To address this need, we used mice with an activatable lung epithelial cell (club cell) specific *Kras*^{G12D} allele (*G12D*) to develop and test a novel model of lung CC. We sought to create a model that more accurately mimics human lung CC in tumor location and burden, rate

of progression and metabolic features. We report that *G12D* mice display classical adipose and skeletal muscle tissue wasting phenotypes of CC over a protracted time course (~12 weeks) and phenocopy tumor and tissue cellular, mutational, transcriptomic, and metabolic characteristics relevant to human lung CC. Exploiting the more protracted time course, we identified adipose tissue wasting as an early event in lung CC. Additionally, circulating biomarkers of fat mobilization observed in *G12D* mice were also apparent in patients with lung cancer and could be reproduced *in vitro* in adipocytes by *G12D* tumor organoid-released factors.

Methods

Animals

The University of Vermont Institutional Animal Care and Use Committee approved animal experiments in compliance with the National Institutes of Health Guidelines for Use and Care of Laboratory Animals. Mice were housed with sex-matched litter mates, with *ad libitum* access to chow and water, except for those housed singly to monitor food intake as described below.

Club cell specific, inducible Kras$^{G12D/+}$ (G12D) mice. G12D (Scgb1a1-CreER^{TM}-Kras$^{LSL-G12D/+}$) or wild-type (Scgb1a1-CreER^{TM}; WT) male and female littermates (4-5 months of age; details in **Supplementary Methods**) were administered 5 consecutive daily intraperitoneal (IP) injections of 20 mg/ml tamoxifen (Sigma-Aldrich, St. Louis, MO, USA) dissolved in corn oil at a dose of 1 mg/10 g body weight. Body weight was measured 2-3 times weekly. Food intake was measured in singly housed mice for 6 weeks. At 6- or 12-weeks post-injection, mice were euthanized by cervical dislocation under pentobarbital anesthesia. Blood was collected by cardiac puncture, centrifuged to isolate serum and stored at -80°C. Skeletal muscles, adipose tissues, and internal organs were weighed, frozen in liquid nitrogen, and stored at -80°C. Lungs were collected for histology or organoid development. One gastrocnemius and soleus muscle were mounted in 7% gum tragacanth, flash-frozen in liquid nitrogen-cooled isopentane, and stored at -80°C. One inguinal (iWAT) and one perigonadal (gWAT) fat pad were fixed in 10% formalin and paraffin-embedded.

Club cell specific, inducible Kras$^{G12D/+}$ -Stk11$^{-/-}$ (KS) mice. G12D mice with a Rosa26-tdTomato reporter (G12D-tm), Kras$^{G12D/+}$- Stk11$^{-/-}$-*tm* (KS-tm), and WT-*tm* mice (8-10 weeks of age; details are in **Supplementary Methods**) were injected (IP) for 5 days with tamoxifen, as detailed for *G12D* mice. Body weight and food intake were monitored thrice weekly for 3.5

weeks, after which mice were euthanized, and blood and tissues were collected similar to *G12D* mice described above.

Lung tumor organoids

Lung tumor or tissue from *G12D* or *WT* mice, respectively, were excised 6 weeks post-tamoxifen injection, and organoid cultures developed, as detailed in **Supplementary Methods**. Maintenance of the oncogenic phenotype was confirmed by assessment of the single nucleotide variant (c.35G>A) in the *Kras* allele via *RNAseq.* Conditioned media (CM) from *G12D* or WT organoids were collected 3 days post organoid passaging and frozen at -80°C. For cell treatment, CM were thawed and diluted 1:3 in cell culture medium.

Cells

3T3-L1-MBX mouse embryonic fibroblasts (ATCC) were cultured and differentiated, as described [21]. All cells were used prior to passage 10 and all experiments were independently replicated 2-3 times.

Human volunteers

Patients recently diagnosed with non-small cell lung cancer (NSCLC; n=7; 5 male, 2 female) and age- and sex-matched healthy controls (HC; n=11; 6 male, 5 female) were recruited, as described [22]. Study details are included in **Supplementary Methods.**

Tumor burden

Hematoxylin and eosin (H&E) stained sections of formalin-fixed, paraffin-embedded lung tissues were imaged and analyzed by a board-certified anatomic pathologist (DJS) blinded to the identity of the specimens. Qupath (v0.3.2) was used to manually annotate tumor vs normal lung tissue and assess tumor burden expressed relative to total lung area (%). The presence of adenocarcinomas was confirmed by a second board-certified anatomic pathologist who was not a member of the research team.

Enzyme-linked immunoassay (ELISA)

Cytokines in organoid CM, cell supernatant, and mouse serum were analyzed using single ELISA and multiplex Luminex assays, as detailed in the **Supplementary Methods**.

Muscle fiber cross-sectional area (CSA)

Sections (10 µm) of gastrocnemius and soleus muscles were stained with H&E, scanned (Leica-Aperio VERSA 8, Leica Biosystems, Deerfield, IL), and 2-3 representative images along the length of the muscle chosen to quantify fiber CSA using ImageJ. Imaging work was performed at the Microscopy Imaging Center at the University of Vermont.

Adipocyte CSA

Sections (4 µm) of iWAT and gWAT were cut, stained with H&E, scanned, and 2-3 representative images across the tissue were used to quantify adipocyte CSA using ImageJ .

RNA isolation and qPCR

Soleus and gastrocnemius muscles, iWAT and gWAT depots, and *G12D* tumor or WT lung tissue organoids were used for RNA isolation (detailed in **Supplementary Methods**). For tissue and cell samples, RNA quality and quantity were assessed (NanoDrop; ThermoFisher Scientific, Waltham, MA, USA) and RNA reverse transcribed using qScript cDNA Supermix (QuantaBio, Beverly, MA, USA). qPCR was performed according to a standard protocol using iTaq Universal SYBR Green Supermix (BioRAD,Hercules, CA, USA) and validated primer sequences (**Supplementary Table S1**). Target gene expression was normalized to two housekeeping genes (adipose: *Ppia, B2m*; muscle: *Gapdh, Ppia*) and expressed as $2^{-\Delta\Delta Ct}$ relative to the housekeeping genes. All data are expressed relative to WT.

RNAseq

RNA libraries were prepared from 500 ng of total RNA using the Zymo-Seq RiboFree Total RNA Library Kit according to the manufacturer's instructions. RNA-Seq libraries were

sequenced on an Illumina NovaSeq to a sequencing depth of at least 30 million read pairs (150 bp paired-end sequencing) per sample. Data were analyzed using the Zymo Research RNA-Seq pipeline, which was adapted from nf-core/rnaseq pipeline v1.4.2 [23] and built using Nextflow [24]. Further details of sequencing and analyses are described in **Supplementary Methods**.

Glycerol levels

Glycerol levels were measured (Sigma-Aldrich MAK117, St Louis, MO, USA), according to manufacturer's instructions.

Statistics

Data were assessed for normality and are reported as mean ± standard error (SEM). Non-normally distributed, were $\log_{10}$-transformed and normality was confirmed prior to analyses. Differences between groups were determined by Student's T-test (WT and *G12D*), analysis of variance (ANOVA; WT, *G12D,* and *KS*) or repeated measures ANOVA for time series data. Statistical control for sex was accomplished using analysis of covariance. *SPSS* (v28) was used for all analyses.

Results:

Lung epithelial cell (club cell) specific Kras^{G12D} induction causes CC.

Induction of the *Kras^{G12D}* allele (**Fig. 1A**) promoted synchronous pulmonary lesions originating in the terminal bronchioles, the anatomic location of club cells (**Fig. 1B**), that ranged from florid bronchial hyperplasia to adenoma to atypical adenomatous hyperplasia to adenocarcinoma at 12 weeks post-induction, with no evidence for dissemination to major organs or lymph nodes. We further examined lung pathology at weight loss initiation (6 weeks post-induction; **Fig. 1C**) and found adenocarcinomas characterized by marked cellular atypia, architecturally distorted glands, the absence of cilia and enhanced mitotic index (**Supplementary Fig. S1A**). In fact, the histologic hallmarks of adenocarcinoma were present, but not as pronounced, as early as 3.5 weeks post-induction (**Supplementary Fig. S1B**). Tumor occupied 22.3% of lung area at 12 weeks post-induction (**Fig. 1B**). To estimate tumor burden, we multiplied tumor fractional area (22.3%) by the weight of the lungs (~200mg for an average mouse in the present study), which resulted in tumor burden of 44.6 mg or ~0.18% of body weight in a 25 gram mouse. We used wild-type, *Scgb1a1-CreER* littermates (WT; *Kras$^{+/+}$*) injected with tamoxifen as controls, which allowed us to control for toxicity and off-target effects of intracellular Cre activation and tamoxifen administration, respectively, and because there was evidence for non-tamoxifen-inducible (*i.e.,* leaky) Cre expression from the CCSP promoter (**Supplementary Fig. S2**). Finally, while tumor development in the lungs could modify body weight regulation via altered lung function, *G12D* mice do not show labored breathing or reduced activity at initiation of body weight loss (6 weeks post-induction), and we found no evidence for systemic hypoxemia prior to onset of body weight loss (**Supplementary Fig. S3A**).

G12D mice achieved an average loss of 15% over 12 weeks (**Fig. 1C**), by which time most animals (83%) displayed cachexia (>10% body weight loss). Weight loss in *G12D* mice was explained by loss of skeletal muscle (gastrocnemius and soleus), white adipose tissue

(iWAT and gWAT), and organ (spleen and liver) weight (**Fig. 1D**), with no group differences in heart weight (**Fig. 1D**) or serum pro-inflammatory cytokines (**Fig. 1E**). Additionally, food intake prior to weight loss initiation (6 weeks) did not differ (**Supplementary Fig. S3B**).

Skeletal muscle and adipose tissue wasting 12 weeks post-induction.

G12D mice exhibited reduced gastrocnemius (**Fig. 2A, Supplementary Fig. S4A**), but not soleus, muscle fiber cross-sectional area (CSA; **Fig. 2A**, **Supplementary Fig. S4B**), with the former showing greater expression of genes involved in protein breakdown and inflammation compared to WT (**Fig. 2B**). In soleus muscle, mRNA levels of *Il6* were greater in *G12D* mice (**Supplementary Fig. S4C**).

Subcutaneous iWAT and visceral gWAT adipocytes exhibited markedly lower CSA at 12 weeks post-induction in *G12D* mice compared to WT mice (**Fig. 2C**), which was accompanied by serum metabolomic evidence of increased fat mobilization and utilization, as indicated by higher levels of circulating short and long-chain fatty acids and markers of carnitine/fatty acid metabolism in *G12D* compared to WT mice (**Supplementary Fig. S5**), and a trend (p=0.06) toward greater circulating glycerol levels (**Fig. 2D**). Consistent with adipocyte wasting, mRNA levels of *Lep* (leptin) were lower in both depots of *G12D* mice (**Fig. 2E**). Moreover, in *G12D* iWAT, mRNA of cytokines *Cxcl1* and *Lif* were greater and the lipid transporter, *Cd36,* and mitochondrial uncoupling marker, *Ucp1,* were lower compared to WT (**Fig. 2E**). In gWAT of *G12D* mice, we observed greater expression of mRNA for the beiging marker, *Cidea*, and trends toward greater expression of genes related to lipolysis, *Cd36* (p=0.06) and *Lipe* (p=0.07 (**Fig. 2E**). Importantly, we investigated sex effects and found that there were no significant differences in the effects of transgene expression in male and female mice for cell size and tissue weights and controlling for sex did not alter our findings. Collectively, these data show that *G12D* mice exhibit tissue, cellular, transcriptomic, and metabolomic hallmarks of CC muscle and adipose tissue wasting.

Early tissue wasting phenotypes in G12D mice.

At 6 weeks post-induction, tumor burden averaged 10.5 ± 1.1% of lung area (**Fig. 3A-B**). Using the calculation approach described for *G12D* mice at 12 weeks, this tumor burden would equate to ~0.084% of body weight. Body weight began to diverge around 3 weeks post-induction but was consistently different at 5 and 6 weeks post-induction (**Fig. 3C**). No differences in skeletal muscle or organ weights were noted between groups 6 weeks post-induction, but *G12D* mice showed markedly lower iWAT and gWAT adipose depot weights (**Fig. 3D**). Moreover, no differences were found in circulating pro-inflammatory cytokines (**Fig. 3E**).

At the cellular level, consistent with skeletal muscle weights (Fig. 3D), neither gastrocnemius nor soleus muscle fiber CSA differed between groups (**Fig. 4A**, **Supplementary Fig. S6A-B**), and except for a trend (p=0.06) toward greater *Fxbxo32* mRNA in the gastrocnemius of *G12D* mice, no differences in muscle gene expression were observed (**Fig. 4B, Supplementary Fig. S6B**). In contrast, adipocytes in both depots showed marked cellular atrophy (**Fig. 4C**) and *G12D* mice had greater circulating glycerol levels compared to WT mice (**Fig. 4D**). Like *G12D* mice, patients with NSCLC showed elevated circulating glycerol levels (**Fig. 4E**). In *G12D* mice, gene expression markers of lipid mobilization were elevated in iWAT compared to WT mice (**Fig. 4F**), with trends towards a similar expression pattern in gWAT (**Fig. 4F**).

In other models of CC, fat wasting is partially explained by the beiging of white adipose tissue. There were no differences in gene expression of markers of beiging at 12 weeks post-induction, aside from an upregulation of *Cidea* in gWAT in *G12D* mice (Fig. 2E), with *Ucp1* mRNA being lower in iWAT from *G12D* compared to WT. At 6-weeks post-induction when weight loss begins and fat loss is the predominant feature of CC, there was a modest (3.2-fold) elevation in mRNA levels of *Ucp1* in iWAT but a trend towards lower expression in gWAT in *G12D* mice (**Fig. 4F**). Using immunohistochemical staining for UCP-1 (**Supplementary Fig S7**),

we found no differences in UCP-1-positive area in either WAT depot (**Supplementary Fig. S8**). Thus, there is no evidence for upregulation of protein expression or regulatory mediators (*i.e., Il-6* mRNA; Fig. 1E and 3E) of white adipose tissue beiging.

Tissue wasting phenotypes in lung club cell specific Kras$^{G12D/+}$-Stk11 null mice.

As patients with lung cancer with mutated *KRAS* lose more weight than patients with wild-type *KRAS* [25], our model is directly relevant to human lung tumor oncotypes that predispose to CC. More recently, studies identified serine/threonine kinase 11 (*STK11*; also known as *LKB1*) mutations as predisposing to CC [26]. We therefore hypothesized that adding club cell specific *Stk11* loss of function (*Stk11$^{-/-}$)* to our *G12D* mouse model should produce a more aggressive form of CC than *G12D* alone. To examine this hypothesis, using our *G12D* mice, we generated mice with combined *Kras$^{G12D/+}$* and *Stk11$^{-/-}$* (*Kras$^{G12D/+}$-Stk11$^{fl/fl}$-tdTomato*; *KS-tm*, **Fig. 5A**). Following tamoxifen injection, *KS-tm* mice exhibited body weight loss over a period of 3.5 weeks (**Fig. 5B**) and diverged from *G12D-tm* and WT-tm littermates 1.5 weeks post-induction independent of differences in food intake (**Fig. 5B**). More rapid weight loss in *KS-tm* mice was coincident with greater tumor burden compared to *G12D-tm* mice (**Fig. 5C**), and weight loss was related primarily to loss of adipose tissue, as no differences in skeletal muscle or organ weights were observed among groups (**Fig. 5D**). *KS-tm* mice had greater circulating levels of IL-6 compared to WT-tm and *G12D-tm* mice compared to WT mice, but no differences in other inflammatory cytokine levels (**Supplementary Fig. S9**). Finally, differences in cell size were consistent with tissue weight data (**Fig. 5E-F**). These data confirm that *Stk11* loss of function predisposes to CC [26], demonstrate the utility of our mouse model to examine the role of lung tumor mutations that may increase susceptibility to CC, and underscore fat wasting as an early feature of lung CC.

Tumor-derived factors that promote CC and adipose tissue wasting.

To examine whether tumor-derived factors initiate adipose tissue wasting, the predominant event in early CC in *G12D* mice, we developed lung tissue and tumor organoids from WT and *G12D* mice, respectively (**Fig. 6A**). Using transcriptomic analysis, we confirmed that the *Kras*^{G12D} mutation present *in vivo* was retained in the cultured *G12D* organoids (**Fig. 6B**). *G12D* lung tumor organoids showed 1076 differentially expressed genes (DEG; 541 upregulated and 535 downregulated) compared to WT lung tissue organoids (**Fig. 6C**), with upregulation of numerous pathways associated with malignancy, including MAPK/KRAS signaling (**Fig. 6D**). As tumor-derived cytokines may contribute to CC [27, 28], we examined differences in inflammatory gene expression between *G12D* tumor and WT lung tissue organoids and found 35 DEG, with 23 upregulated and 12 downregulated (**Supplementary Fig. S10A**). None of the differentially expressed pro-inflammatory genes have been previously implicated in the pathogenesis or progression of CC based on findings in preclinical models, except *Gdf15* [29], which was elevated in *G12D* organoids. Despite upregulation of *Gdf15* in *G12D* organoids, no elevation of GDF-15 protein level was measured in serum from *G12D* mice at either 6- or 12 weeks following induction (Fig. 3E and 1E, respectively). Thus, we found no evidence for upregulation of inflammatory cytokines associated with CC in *G12D* tumor organoids.

To determine whether tumor-derived factors might incite CC in *G12D* mice, cultured 3T3-L1 adipocytes were treated with conditioned media (CM) collected from WT or *G12D* organoids (**Fig. 7A**) and lipolysis assessed by measuring media glycerol levels. Treatment of adipocytes with *G12D* organoid CM for 24 hours increased media glycerol levels compared to WT organoid CM (**Fig. 7B**), and this was not due to increased glycerol levels in *G12D* CM (**Fig. 7C**). Treatment of 3T3-L1 adipocytes with *G12D* CM also increased media pro-inflammatory cytokine levels compared to WT CM (**Fig. 7D**), and this was not attributable to differences in cytokine levels between *G12D* and WT organoid CM (**Fig. 7E**). Thus, *G12D* tumor organoids

release factors that increase adipose tissue lipolysis, the metabolic pathway contributing to adipose tissue depletion in human CC [30].

Discussion:

Questions about the translational relevance of traditional pre-clinical models [8, 9, 12, 13] have led many laboratories to develop new animal models of CC [31-34]. Most of these new models have focused on pancreatic CC [31, 32], which is logical given the prevalence and severity of CC in patients with pancreatic cancer. Lung cancer also has high rates of CC [16, 17] and is the leading cause of cancer-related deaths worldwide [15]. We report the development of a new model of lung CC using mice with a lung epithelial specific, tamoxifen inducible *Kras*^{G12D} mutation. *G12D* mice exhibit more physiologically relevant tumors with respect to their anatomic location and burden, a slower time course of CC initiation and progression, and morphological, mutational, transcriptomic, and metabolic characteristics that parallel CC in patients with lung cancer.

Tumor location, burden, and mutations

Most studies of CC have employed heterotopic murine models, in which tumor cells are injected into the flank, producing a tumor akin to a metastatic lesion but in an atypical microenvironment (i.e., subcutaneous). Recent studies have advanced this approach by administering cancer cells into the vasculature to seed tumors in the lung [33, 34]. In *G12D* mice, the transgene is targeted to lung epithelial cells, and tumors originate in the terminal bronchioles, the anatomic location of most lung tumors in humans [35]. At the initiation of weight loss (6 weeks post-induction), tumor burden in *G12D* mice is much smaller (<0.1% of body weight) than heterotopic lung CC models (~5% of body weight [19]), better reflecting tumor burden in human patients. An additional advantage of *G12D* mice is that *KRAS* is the most frequently mutated oncogene in human NSCLC [36], and patients that have lung tumors with mutated *KRAS* experience greater weight loss [25]. Building on recent reports suggesting that *STK11* loss-of-function amplifies lung CC in humans [26], our data also demonstrate that mice with combined *Kras*^{G12D}/*Stk11*$^{-/-}$ develop a more rapidly progressive CC compared to *Kras*^{G12D}

alone. Thus, inducible, lung epithelial cell specific expression of *G12D* offers a model that better approximates tumor characteristics in human lung CC with respect to anatomic location, burden, and mutations that predispose to CC.

CC initiation and progression

Available lung CC models show rapid onset and progression of weight loss. For example, in the LLC model, weight loss progresses rapidly such that euthanasia is often required within 3-4 weeks of the injection of tumor cells [19]. While recent lung CC models have advanced the LLC model to localize tumors to the lungs [33, 34], they still exhibit rapid onset and progression of weight loss. The rapidity of weight loss in these models does not reflect what occurs in patients and makes it difficult to define pathoetiological factors contributing to CC. In contrast, the initiation and progression of weight loss in *G12D* mice is slower, with an ~4-6-week latency following $Kras^{G12D}$ induction until weight loss begins, followed by progressive weight loss until 12 weeks post-induction. The relatively slow rate of weight loss in *G12D* mice after initiation (~1.9%/week) more closely approximates that in patients with lung cancer [37] and offers a comparatively longer time to test the efficacy of therapeutics (~6-8 weeks).

Systemic inflammation

While systemic inflammation has long been hypothesized to contribute to CC initiation and progression, more recent work in patients with pancreatic cancer has questioned this notion [10, 11]. Our results agree with these data from patients, as we found no evidence of increased circulating levels of inflammatory cytokines in *G12D* mice, but contrast the profound systemic inflammation present in the LLC and other preclinical models of CC [28, 38]. Moreover, while studies suggest that inflammation may be driven by tumor-secreted cytokines [27, 39], recent data from tumors of patients with lung cancer with or without cachexia showed no differential expression of pro-inflammatory cytokine genes [40]. In agreement with these human data, in tumor organoids developed from *G12D* mice, we found no evidence for upregulation of mRNA

for classical inflammatory mediators of CC and no increased secretion of pro-inflammatory cytokines into organoid media compared to non-tumor lung organoids. We did find increased mRNA levels for *Gdf15* in *G12D* tumor organoids, but no elevation of GDF-15 in the circulation of these mice. In contrast, we found evidence for upregulation of cytokine expression in fat and muscle tissue. The precise role of local versus systemic inflammatory cytokines in human CC, however, remains unclear.

Early adipose tissue wasting

Exploiting the more protracted time course of the *G12D* mouse model, we report early wasting of adipose tissue in both *G12D* and *Kras*$^{G12D/+}$-*Stk11*$^{-/-}$ mice, the latter of which exhibit more rapid weight loss. Whether early adipose tissue wasting is apparent in patients with lung cancer is unclear, although recent prospective data from the TRACERx cohort, which included mostly early-stage NSCLC (I-III), showed that of those patients losing tissue mass, 78% experienced fat loss in the presence or absence of muscle loss between their primary diagnosis and disease relapse, with 43% of patients experiencing only fat loss, underscoring the predominance of fat loss in patients with lung cancer [40]. Additionally, prospective data in patients with pancreatic cancer showed that the relative loss of adipose tissue was twice that of skeletal muscle and, in turn, was a stronger predictor of body weight loss [41]. Nonetheless, we acknowledge that the timing, magnitude, and composition of tissue wasting may differ between cancer types, sub-types, and/or the microenvironments where tumors are located. Patients with a variety of cancers experience weight loss prior to diagnosis, including those with lung cancer [37], and further studies examining early body composition changes in patients with lung cancer are needed to clarify whether early adipose tissue wasting in *G12D* mice translates to humans or is a general feature of CC.

Factors released from *G12D* tumors may contribute to early adipose tissue wasting, as we found that cultured adipocytes treated with *G12D* tumor organoid CM release greater

amounts of glycerol into the media, a proxy of lipolysis, compared to adipocytes treated with WT lung tissue organoid CM. These effects of tumor organoid-derived factors may model CC *in vivo*, as we found increased circulating glycerol levels in *G12D* mice at 6 weeks post-induction, when adipose tissue loss is apparent and weight loss begins. In fact, trends towards elevated circulating glycerol were apparent at 12 weeks post-induction, when adipose tissue was profoundly depleted. Evidence that elevated lipolysis translates to human patients is provided by our data showing elevated glycerol levels in patients with NSCLC compared to non-cancer controls, and studies in patients with gastrointestinal cancer showing that the lipolytic response in isolated adipocytes was increased in patients with cachexia compared to those without cachexia [30]. Thus, early adipose tissue wasting may be an early pathophysiological hallmark of CC and organoids from *G12D* mice may provide an *in vitro* experimental model to study tumor-released factors that initiate CC-associated adipose tissue wasting.

Conclusions

Our data show that the *G12D* mouse model phenocopies tissue, cellular, mutational, transcriptomic, and metabolic characteristics of human CC. Additionally, because of the protracted time course for initiation and progression of CC relative to other pre-clinical lung CC models, *G12D* mice are well-suited to both identify mechanisms leading to CC and test preventative and remediative therapies. Finally, we identify adipose tissue wasting as an early event in this and other *Kras*-driven mouse models of lung CC that may be attributable to tumor-released factors.

Acknowledgements:

This study was funded by NIH R01 AR065826 (MJT), R21 CA283492 (MJT), T32 HL076122 (MEP), R21 CA280266 (DJS), R01 CA273238 (YJ-H) and the University of Vermont Cancer Center. The University of Colorado SOM Metabolomics Core is supported in part by the University of Colorado Cancer Center via NIH P30CA046934. Funding in support of RNAseq was provided by a Zymo Impact Initiative Grant (DBS). The authors thank Vikas Anathy and Zoe Mark for the machinery and technical support needed to measure oxygen saturation (**Supplementary Fig. S3A**).

Author Contributions

Conceptualization: MJT, DBS; Methodology: DBS, MEP, DM, DJS, YJH; Validation: DBS ; Formal analysis: DBS, DM, JSD; Investigation: DBS, JLA, JV, SML, HS, ERB, SCJH, DS, JAR; Resources: MJT, MEP, JV, DM, DJS, YJH, AD; Data Curation: DBS, HS, ERB, SCJH, SML, DS; Writing- original draft preparation: DBS, MJT; Writing- review and editing: all authors; Visualization: DBS; Supervision: MJT, MEP, DJS, DBS; Project administration: DBS and MJT; Funding acquisition: MJT, MEP, YJ-H and DBS.

Declaration of Interests: The authors declare no conflicts of interest.

Figure Titles and Legends

Fig. 1. Characterization of lung club cell specific, inducible Kras$^{G12D/+}$ (G12D) mice at 12 weeks post-induction.

G12D mice harbor a tamoxifen (TAM)-inducible, lung club cell specific *Kras^{G12D}* mutation under the control of the club cell secretory protein (CCSP) promoter (A). Four- to 5-month-old mice received intraperitoneal tamoxifen (TAM), which led to progressive, reproducible, and synchronous lesions in lung bronchioles by 12 weeks post-induction compared to wild-type (WT) mice that ranged from florid bronchial hyperplasia to adenocarcinoma (B). Body weight change relative to Day 0 (C), skeletal muscle, fat pad and organ weights (D) and serum pro-inflammatory cytokines (interleukin 6 (IL-6), soluble IL-6 receptor alpha (IL-6Rα), tumor necrosis factor alpha (TNFα), CXC motif ligand 1 (CXCL1/KC), growth differentiation factor 15 (GDF-15), monocyte chemoattractant protein 1/C-C motif ligand 2 (MCP-1/CCL2), CXCL10, and interleukin-1 beta (IL-1β)) in wild-type (WT; n=7; blue bars/lines) and G12D mice (n=6; gold bars/lines)(E). Data were analyzed using repeated measures analysis of variance (C) or Student's t-test (D, E), with asterisks indicating significance: * $p<0.05$, ** $p<0.01$, and *** $p<0.001$. Note that n=5-7/group for serum cytokine measures due to limited serum collection from some mice. Image created with Biorender.com (A).

Fig. 2. Effect of lung club cell specific, inducible Kras$^{G12D/+}$ (G12D) on skeletal muscle and adipose tissue wasting and mRNA expression at 12-weeks post-induction.

Gastrocnemius (gastroc) and soleus muscle fiber cross-sectional area (CSA) 12 weeks post-induction in wild-type (WT; n=7; blue bars) and *G12D* mice (n=6; gold bars) and representative images of gastrocnemius muscle sections used for quantification (scale bars=100 μm) (A). mRNA levels for markers of protein degradation and inflammatory cytokines in gastrocnemius muscle, expressed as $2^{-\Delta\Delta CT}$ relative to the WT group (B). CSA of adipocytes from inguinal white

adipose tissue (iWAT) and gonadal WAT (gWAT) depots in WT (n=7) and *G12D* (n=6) mice and images of representative tissue sections used for quantitation (scale bars= 100 µm) (C). Serum glycerol levels in WT and *G12D* mice standardized to body mass (D). Gene expression of iWAT and gWAT depots for markers of lipid balance, inflammation, and beiging (E). Data were analyzed by Student's t-test with asterisks indicating * $p<0.05$ and *** $p<0.001$. Significance values where $p>0.05$, but <0.10 are indicated above specific data.

Fig. 3. Characterization of lung club cell specific, inducible Kras$^{G12D/+}$ (G12D) murine model of CC at 6-weeks post-induction.

Representative lung cross-section of a *G12D* mouse (A) and average tumor burden (percent tumor area / total lung area) (B). Body weight change relative to Day 0 in wild-type (WT; n=7; blue lines/bars) and *G12D* (n=8; gold lines/bars) mice (C). Hindlimb muscle, fat pad, and organ weights of 6-week WT and *G12D* mice at necropsy (D). Serum levels of pro-inflammatory cytokines in 6-week mice (E). Data were analyzed by repeated measures analysis of variance (C) and Student's t-tests (D, E), with significance denoted as ** $p<0.01$ and *** $p<0.001$. Significance values $p>0.05$ but <0.10 are indicated above specific data.

Fig. 4. Effect of lung club cell specific, inducible Kras$^{G12D/+}$ (G12D) on skeletal muscles and adipose tissues 6 weeks post-induction.

Mean muscle fiber cross-sectional area (CSA) in gastrocnemius and soleus muscles of wild-type (WT; n=7; blue bars) and *G12D* (n=8; gold bars) mice were assessed 6 weeks post tamoxifen injection, with representative images of WT and *G12D* muscle used for quantification of fiber CSA (scale bars=100 µm) (A). Gene expression in gastrocnemius muscle, represented as $2^{-\Delta\Delta CT}$ compared to WT mice (B). Cross-sectional area (CSA) of adipocytes from inguinal (iWAT) and perigonadal (gWAT) white adipose tissue depots in 6-week WT and *G12D* mice,

with representative images of sections used for cell size quantitation (scale bars=100 µm) (C). Glycerol levels standardized to body mass in WT and *G12D* mice (D), and in plasma of patients with late-stage, non-small cell lung cancer (NSCLC; n=7; purple bar) after 2 months of treatment compared to healthy controls (n=11; black bar) without current or prior history of cancer (E). Gene expression was assessed in iWAT and gWAT of *G12D* and WT mice for genes related to lipid balance, inflammation, and beiging (F). Data were analyzed Student's t-test with asterisks indicating * $p<0.05$ and ** $p<0.01$. Significance values where $p>0.05$ but <0.10 are indicated above specific data.

Fig. 5. Comparison of lung club cell specific, inducible Kras$^{G12D/+}$ (G12D-tm) and Kras^{G12D}/Stk11$^{-/-}$ (KS-tm) mice.

KS-tm mice harbor an additional tamoxifen (TAM)-inducible lung club cell specific deletion of *Stk11/Lkb1* and a *Rosa26-tdTomato* reporter (A). Percent change in body weight and cumulative food intake (B) and tumor burden (C) of wild-type (WT-tm; n=4; blue lines/open blue bars), *G12D-tm* (n=5; gold lines/open gold bars) and *KS-tm* (n=5; red lines/open red bars) mice injected with tamoxifen or vehicle at 9-10 weeks of age and studied 24 days post-induction. Organ, muscle, fat pad and organ weights at necropsy (D). Mean gastrocnemius (Gastroc) muscle fiber (E) and iWAT and gWAT adipocyte (F) CSA. Data were analyzed using a repeated measures ANOVA (B), Student's t-test (C), or a one-way ANOVA (B, D-F) with post hoc comparisons for ANOVAs for those with $p<0.05$ group or group X time interaction effects, with ** $p<0.01$ and different letters indicating differences by post hoc comparisons. Image created with BioRender.com (A).

Fig. 6. Organoids developed from lung tissue from wild-type (WT) and lung tumors from $Kras^{G12D/+}$ (G12D) mice and their characterization.

Lung organoid development with representative images of wild-type (WT; blue) and *G12D* (gold) organoids (A; scale bars = 250 μm). *RNAseq* was used to validate the presence of the $Kras^{G12D}$ mutation, shown in gold, in *G12D* lung tumor organoids (B). Volcano plot depicting differentially expressed genes, with red representing upregulated (n=535) and blue representing downregulated (n=541) genes, respectively, in *G12D* organoids compared to WT organoids, with a *p*-value exclusion of 0.05 (C). Pathway analysis using PATHFINDR depicting upregulated signaling pathways in *G12D* lung tumor organoids in comparison with WT lung tissue organoids (D). Images created with BioRender.com (A-B).

Fig. 7. Conditioned media (CM) from $Kras^{G12D/+}$ (G12D) lung tumor organoids promotes lipolysis in cultured 3T3-L1 adipocytes.

CM was collected from wild-type lung tissue (WT; blue circles) or *G12D* tumor (gold squares) organoid cultures, respectively, and applied (1:3 with adipocyte culture media) to fully differentiated 3T3-L1 adipocytes (A). Glycerol levels of supernatant of 3T3-L1 adipocytes treated with WT (blue circles) or *G12D* (gold squares) organoid CM for 24 h (B). CM glycerol levels collected from WT and *G12D* organoids (C). Supernatant levels of IL-6, MCP-1, and CXCL1 from 3T3-L1 adipocytes treated for 24 hours with WT or *G12D* organoid CM (D), and CM levels of these cytokines (E). 3T3-L1 experiments are representative of 2-3 independent replicates. Note that replicates for CM assessments in panels C and E reflect testing of different aliquots of CM used for experiments from WT and *G12D* organoid cultures. Student's t-tests were used to determine significant differences among groups, with *** $p<.001$. Images created with BioRender.com (A-E).

References:

1. Fearon, K., et al., *Definition and classification of cancer cachexia: An international consensus.* Lancet Oncol, 2011. **12**(5): p. 489-95.
2. Miyawaki, T., et al., *Desensitizing effect of cancer cachexia on immune checkpoint inhibitors in patients with advanced nsclc.* JTO Clin Res Rep, 2020. **1**(2): p. 100020.
3. Kurk, S., et al., *Skeletal muscle mass loss and dose-limiting toxicities in metastatic colorectal cancer patients.* J Cachexia Sarcopenia Muscle, 2019. **10**(4): p. 803-813.
4. Dewys, W.D., et al., *Prognostic effect of weight loss prior to chemotherapy in cancer patients.* Am J Med, 1980. **69**: p. 491-497.
5. Reeve, B.B., et al., *Impact of cancer on health-related quality of life of older americans.* J Natl Compr Canc Netw, 2009. **101**(12): p. 860-868.
6. Ross, P.J., et al., *Do patients with weight loss have a worse outcome when undergoing chemotherapy for lung cancers?* Br J Cancer, 2004. **90**(10): p. 1905-11.
7. Fearon, K.C.H., D.J. Glass, and D.C. Guttridge, *Cancer cachexia: Mediators, signaling and metabolic pathways.* Cell Metab, 2012. **16**: p. 1-14.
8. Baracos, V.E., *Bridging the gap: Are animal models consistent with clinical cancer cachexia?* Nat Rev Clin Oncol, 2018. **15**(4): p. 197-198.
9. Johns, N., N.A. Stephens, and K.C. Fearon, *Muscle wasting in cancer.* Int J Biochem Cell Biol, 2013. **45**(10): p. 2215-29.
10. Ramsey, M.L., et al., *Circulating interleukin-6 is associated with disease progression, but not cachexia in pancreatic cancer.* Pancreatology, 2019. **19**(1): p. 80-87.
11. Talbert, E.E., et al., *Circulating monocyte chemoattractant protein-1 (mcp-1) is associated with cachexia in treatment-naïve pancreatic cancer patients.* J Cachexia Sarcopenia Muscle, 2018. **9**(2): p. 358-368.

12. Tomasin, R., A.C.B.M. Martin, and M.R. Cominetti, *Metastasis and cachexia: Alongside in clinics, but not so in animal models.* J Cachexia Sarcopenia Muscle, 2019. **10**(6): p. 1183-1194.

13. Mueller, T.C., et al., *Molecular pathways leading to loss of skeletal muscle mass in cancer cachexia – can findings from animal models be translated to humans?* BMC Cancer, 2016. **16**(1): p. 75.

14. Ferrer, M., et al., *Cachexia: A systemic consequence of progressive, unresolved disease.* Cell, 2023. **186**(9): p. 1824-1845.

15. Siegel, R.L., et al., *Cancer statistics, 2023.* Cancer J Clin 2023. **73**(1): p. 17-48.

16. Bozzetti, F., *Forcing the vicious circle: Sarcopenia increases toxicity, decreases response to chemotherapy and worsens with chemotherapy.* Ann Oncol, 2017. **28**(9): p. 2107-2118.

17. Baracos, V.E., et al., *Body composition in patients with non–small cell lung cancer: A contemporary view of cancer cachexia with the use of computed tomography image analysis.* Am J Clin Nutr, 2010. **91**(4): p. 1133S-1137S.

18. Miyawaki, T., et al., *Predicting the efficacy of first-line immunotherapy by combining cancer cachexia and tumor burden in advanced non-small cell lung cancer.* Thorac Cancer, 2022. **13**(14): p. 2064-2074.

19. DeWys, W.D., *Studies correlating the growth rate of a tumor and its metastases and providing evidence for tumor-related systemic growth-retarding factors.* Cancer Res, 1972. **32**(2): p. 374-9.

20. Lee, J., et al., *Longitudinal changes in skeletal muscle mass in patients with advanced squamous cell lung cancer.* Thorac Cancer, 2021. **12**(11): p. 1662-1667.

21. Ather, J.L., et al., *Obese adipose tissue modulates proinflammatory responses of mouse airway epithelial cells.* Am J Physiol Regul Integr Comp Physiol, 2021. **321**(1): p. R79-r90.

22. Snoke, D.B., et al., *Skeletal muscle adaptations in patients with lung cancer: Longitudinal observations from the whole body to cellular level.* J Cachexia Sarcopenia Muscle, 2023.

23. Patel, H., et al., *Nf-core/rnaseq: Nf-core/rnaseq v3.0 - silver shark (version 3.0)*. 2020, Zenodo.

24. Di Tommaso, P., et al., *Nextflow enables reproducible computational workflows.* Nat Biotechnol, 2017. **35**(4): p. 316-319.

25. Shiono, M., et al., *An analysis of the relationship between metastases and cachexia in lung cancer patients.* Cancer Med, 2016. **5**(9): p. 2641-8.

26. Iyengar, P., et al., *Tumor loss-of-function mutations in stk11/lkb1 induce cachexia.* JCI Insight, 2023. **8**(8).

27. Rupert, J.E., et al., *Tumor-derived il-6 and trans-signaling among tumor, fat, and muscle mediate pancreatic cancer cachexia.* J Exp Med, 2021. **218**(6).

28. Baltgalvis, K.A., et al., *Interleukin-6 and cachexia in apcmin/+ mice.* Am J Physiol Regul Integr Comp Physiol, 2008. **294**(2): p. R393-R401.

29. Suriben, R., et al., *Antibody-mediated inhibition of gdf15-gfral activity reverses cancer cachexia in mice.* Nat Med, 2020. **26**(8): p. 1264-1270.

30. Ryden, M., et al., *Lipolysis--not inflammation, cell death, or lipogenesis--is involved in adipose tissue loss in cancer cachexia.* Cancer, 2008. **113**(7): p. 1695-704.

31. Talbert, E.E., et al., *Modeling human cancer-induced cachexia.* Cell Rep, 2019. **28**(6): p. 1612-1622.e4.

32. Go, K.L., et al., *Orthotopic patient-derived pancreatic cancer xenografts engraft into the pancreatic parenchyma, metastasize, and induce muscle wasting to recapitulate the human disease.* Pancreas, 2017. **46**(6): p. 813-819.

33. Arneson-Wissink, P.C., A.M. Ducharme, and J.D. Doles, *A novel transplantable model of lung cancer-associated tissue loss and disrupted muscle regeneration.* Skelet Muscle, 2020. **10**(1): p. 6.

34. van de Worp, W., et al., *A novel orthotopic mouse model replicates human lung cancer cachexia.* J Cachexia Sarcopenia Muscle, 2023. **14**(3): p. 1410-1423.

35. Chen, Z., et al., *Non-small-cell lung cancers: A heterogeneous set of diseases.* Nature Rev Cancer, 2014. **14**(8): p. 535-546.

36. Judd, J., et al., *Characterization of kras mutation subtypes in non–small cell lung cancer.* Mol Cancer Ther, 2021. **20**(12): p. 2577-2584.

37. Gannavarapu, B.S., et al., *Prevalence and survival impact of pretreatment cancer-associated weight loss: A tool for guiding early palliative care.* J Oncol Pract, 2018. **14**(4): p. e238-e250.

38. Au, E.D., et al., *The mek-inhibitor selumetinib attenuates tumor growth and reduces il-6 expression but does not protect against muscle wasting in lewis lung cancer cachexia.* Front Physiol, 2017. **7**.

39. Lerner, L., et al., *Map3k11/gdf15 axis is a critical driver of cancer cachexia.* J Cachexia Sarcopenia Muscle, 2016. **7**(4): p. 467-482.

40. Al-Sawaf, O., et al., *Body composition and lung cancer-associated cachexia in tracerx.* Nat Med, 2023. **29**(4): p. 846-858.

41. Babic, A., et al., *Adipose tissue and skeletal muscle wasting precede clinical diagnosis of pancreatic cancer.* Nat Commun, 2023. **14**(1): p. 4317.

Fig. 1. Characterization of lung club cell-specific, inducible Kras$^{G12D/+}$ (G12D) mice at 12 weeks post-induction.

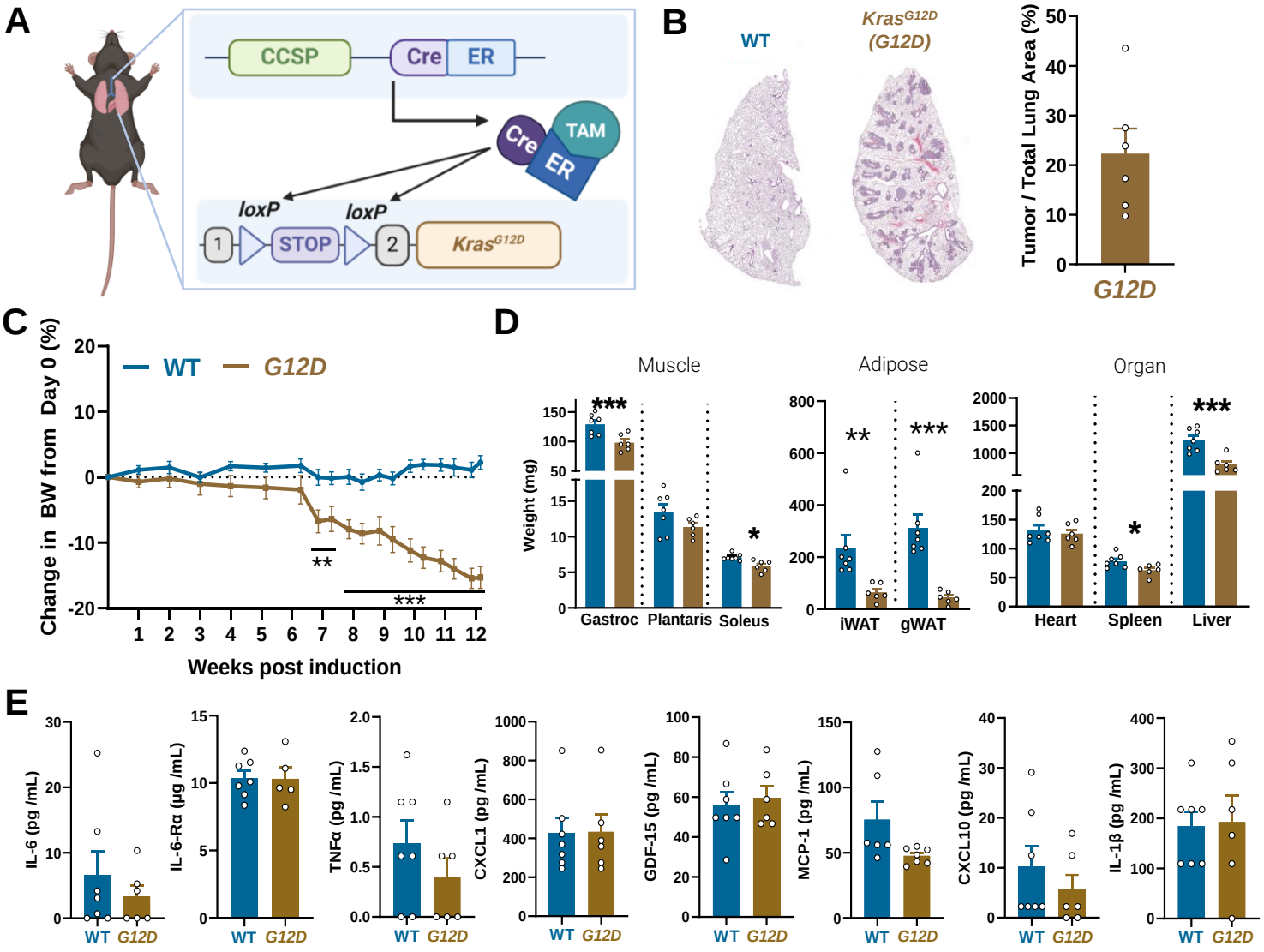

Figure 2. Effect of lung club cell-specific, inducible Kras$^{G12D/+}$ (G12D) on skeletal muscle and adipose tissue wasting and mRNA expression at 12-weeks post-induction.

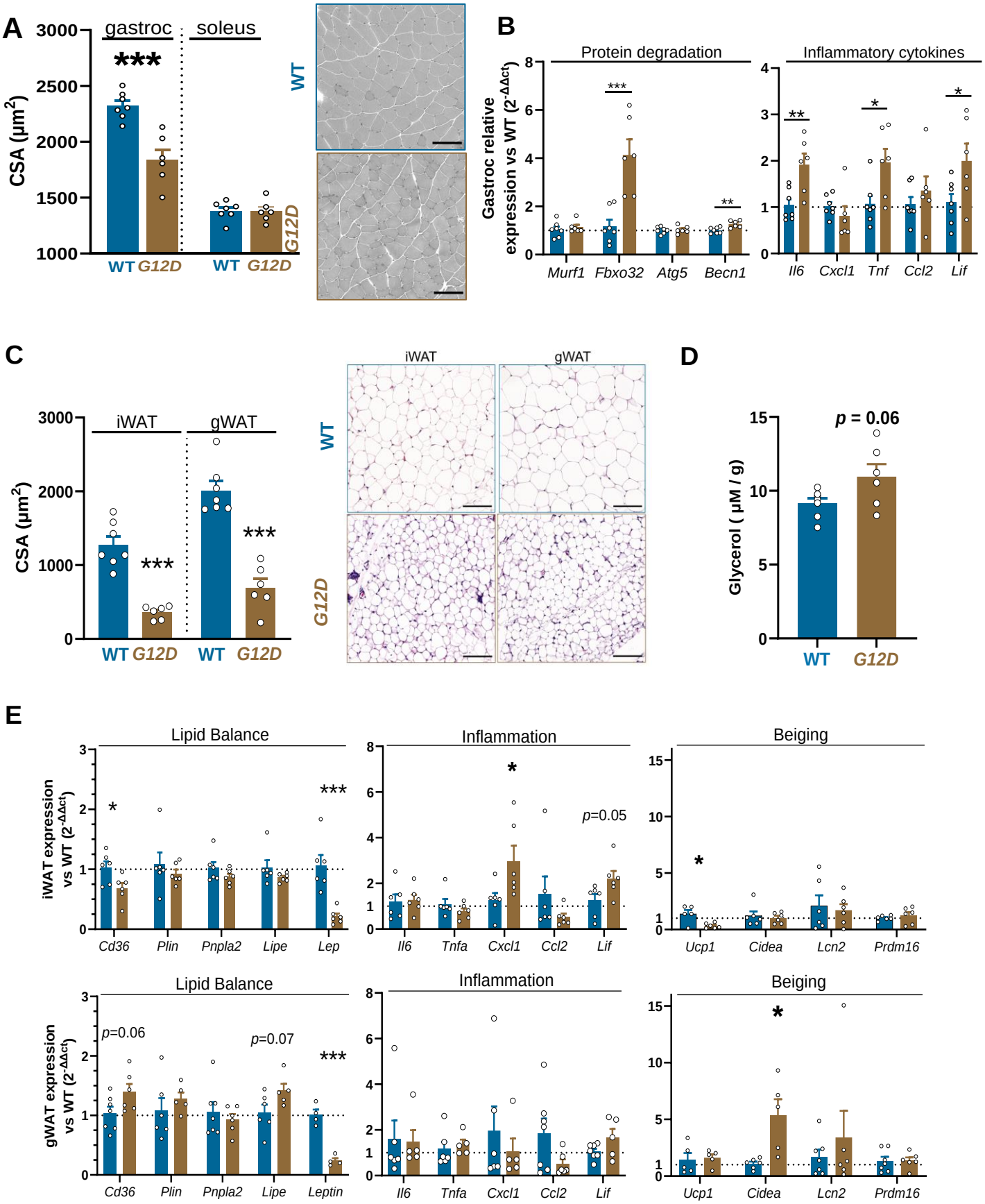

Figure 3. Characterization of lung club cell-specific, inducible Kras$^{G12D/+}$ (G12D) murine model of CC at 6-weeks post-induction

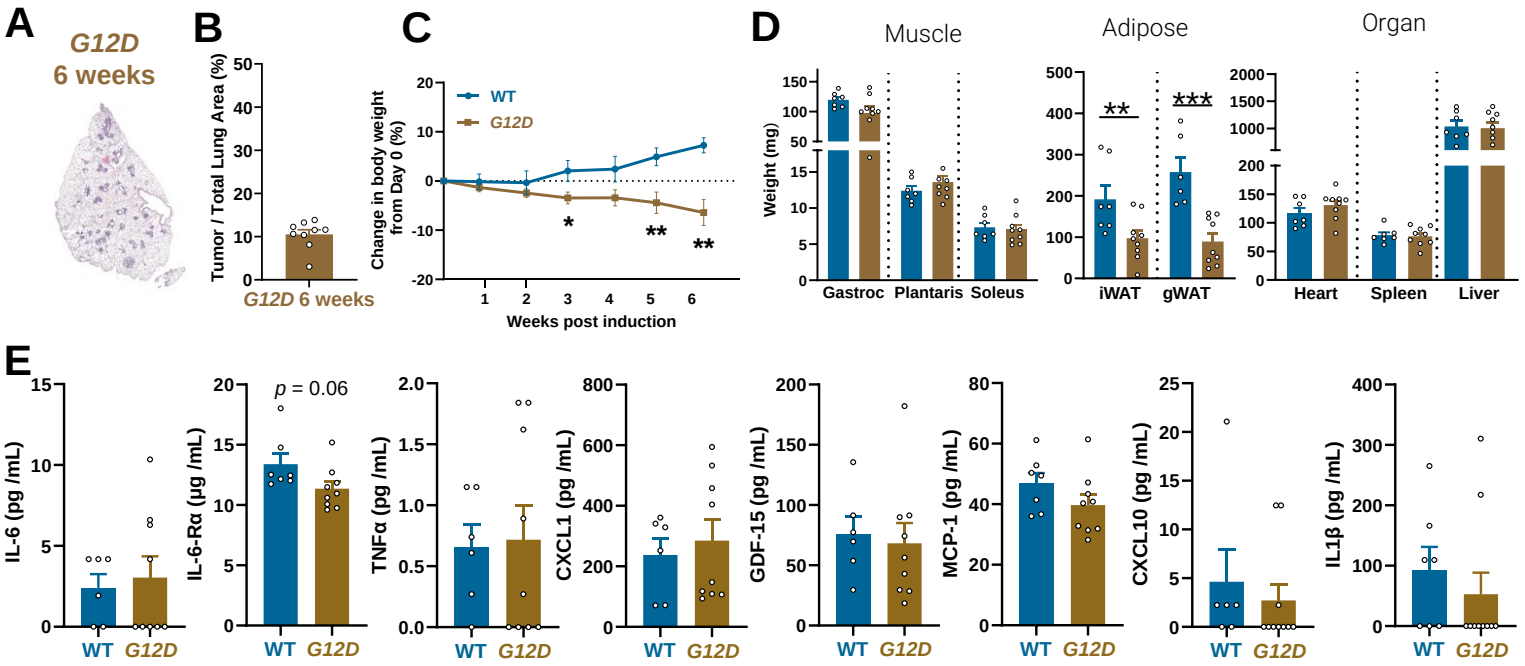

Figure 4. Effect of lung club cell-specific, inducible Kras$^{G12D/+}$ (G12D) on skeletal muscles and adipose tissues 6 weeks post-induction

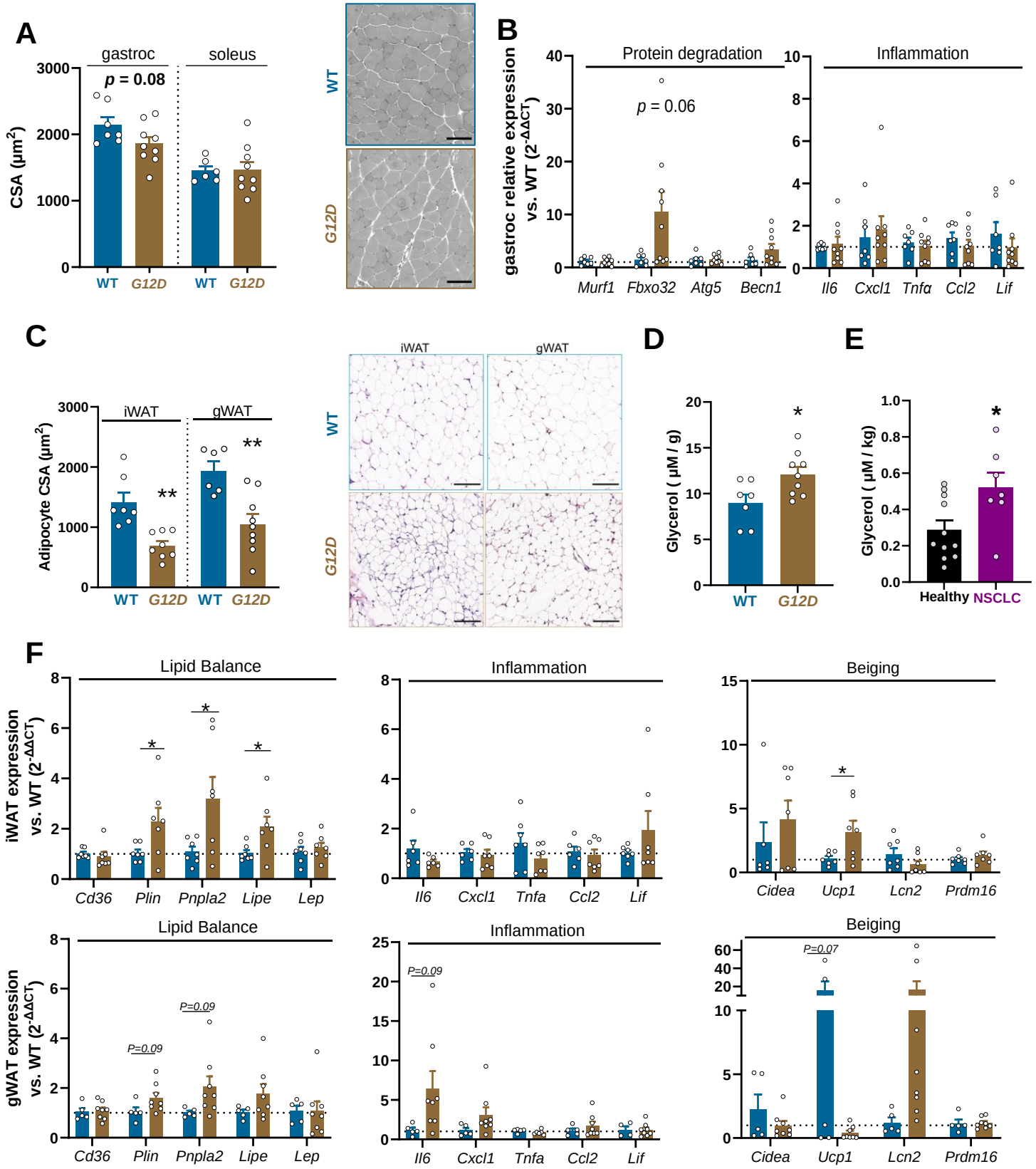

Figure 5. Comparison of lung club cell-specific, inducible Kras$^{G12D/+}$ (G12D-tm) and Kras$^{G12D/+}$-Stk11$^{-/-}$ (KS-tm) murine models of CC.

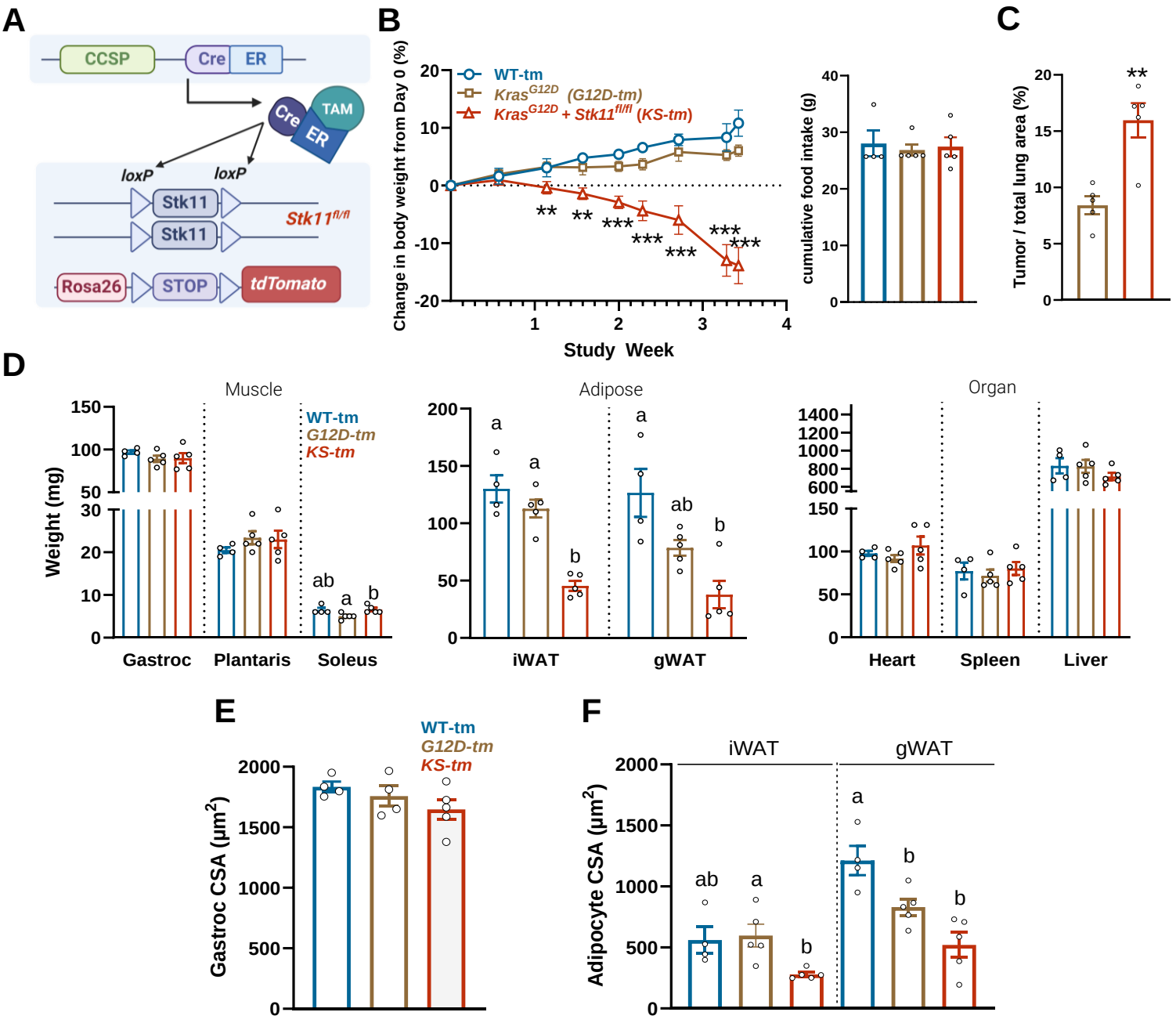

Figure 6. Organoids developed from lung tissue from wild type (WT) and lung tumors from Kras$^{G12D/+}$ (G12D) mice and their characterization.

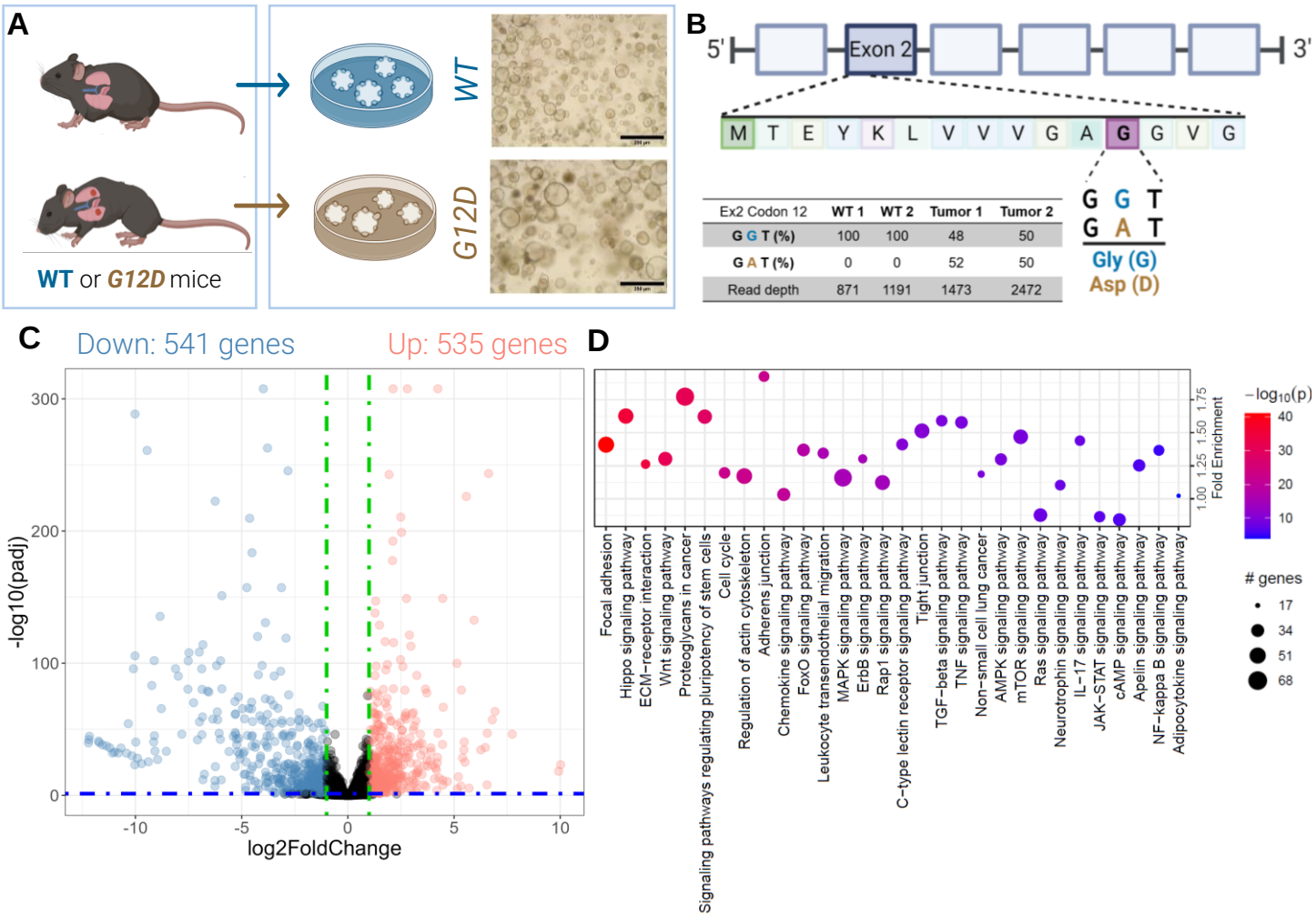
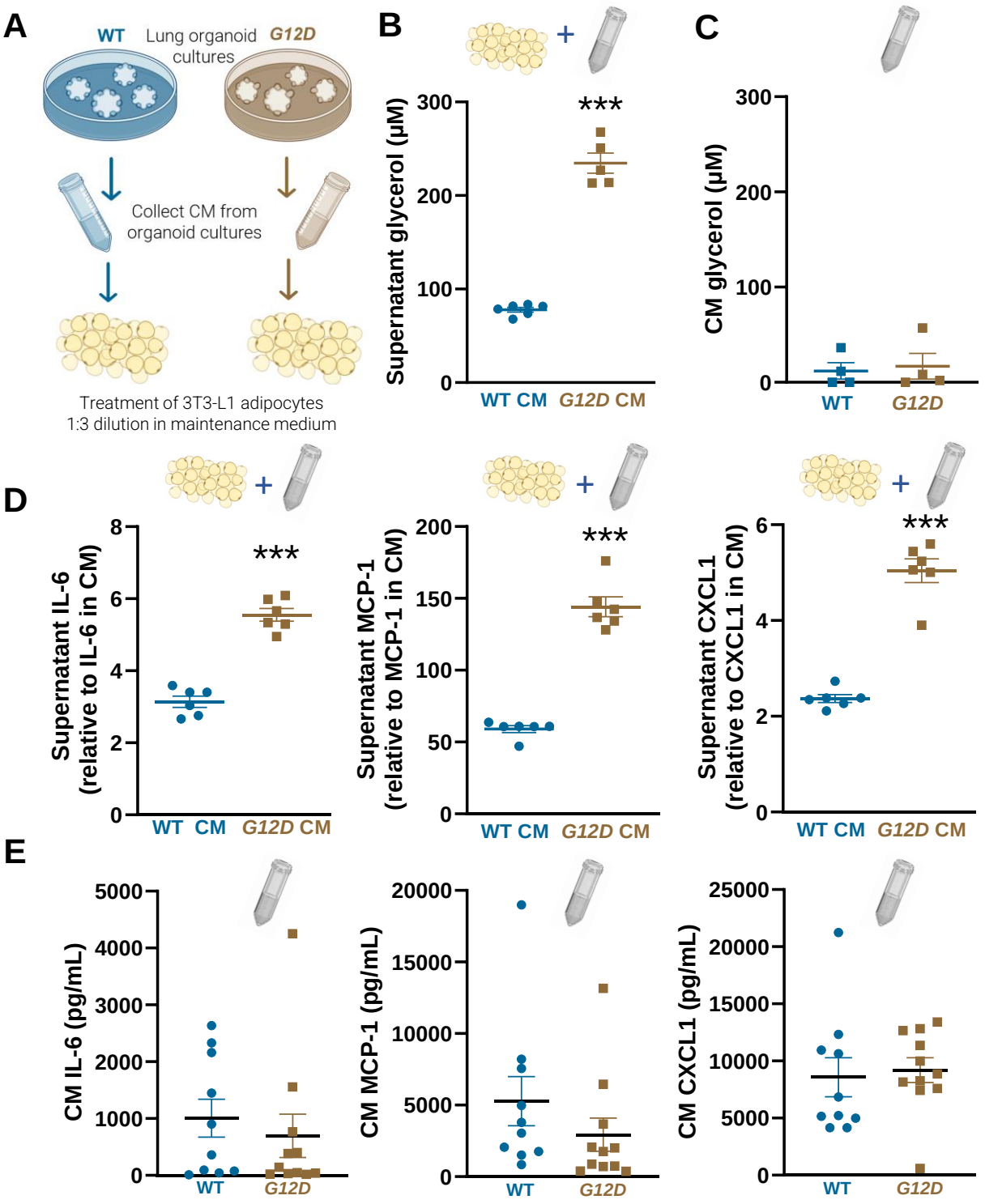
Figure 7. Conditioned media (CM) from Kras$^{G12D/+}$ (G12D) lung tumor organoids promotes lipolysis in cultured 3T3-L1 adipocytes.